Effect of Compressibility on Performance of Hydraulic Wash Columns

L. van Oord-Knol, O. S. L. Bruinsma, and P. J. Jansens
Laboratory for Process Equipment, Delft University of Technology, 2628 CA Delft, The Netherlands

In a hydraulic wash column the solid crystals are separated from the mother liquor by filtration in the top section of the column. Remaining impurities are removed via countercurrent washing of the crystals in the bottom section. Since compressibility limits the capacity of a wash column, this phenomenon needs to be quantified and modeled rigorously. The compressibility of the bed was determined from the porosity profile and the liquid-pressure profile inside the wash column. The porosity of the bed decreases from 0.65 to 0.3 during transport of the bed. This is associated with a decrease in local bed permeability by a factor of 10. The compressibility of the bed, therefore, partly explains the large ratio between the average permeability above and below the wash front. Compressibility coefficients make it possible to relate the compressive stress to the porosity and permeability in the top section of the bed. These coefficients are, therefore, incorporated in a model to successfully predict the capacity of a wash column with a compressible bed.

Introduction

Melt crystallization processes can be used for the ultrapurification of organic compounds at a relatively low energy consumption compared to the distillation processes, while the use of solvents such as in liquid extraction processes is avoided. When appropriate growth rates are applied, highly pure crystals can be formed in suspension crystallization processes. To reach the desired purity of the end product, the crystals have to be separated from the impure mother liquor and washed to remove any adhering mother liquor. This solid–liquid separation and washing can be performed in so-called wash columns. Three types of wash columns can be named according to the transport mechanism of the solids: gravitational, mechanical, and hydraulic. Industrial designs of all three types are discussed in the literature. In hydraulic wash columns transportation of the packed bed is due to the liquid pressure drop over the bed (Arkenbout, 1995).

The working mechanism of the TNO-Thijssen-type hydraulic wash column is illustrated in Figure 1. A feed slurry is pumped into the top of the wash column, which is a cylinder containing one or more vertical filter tubes. The mother liquor and the crystals move through a short slurry zone until a packed bed of crystals is reached. The crystals fall on top of the bed, while the mother liquor flows through the packed bed to filters positioned in the filter tubes. The mother liquor leaves the column via the filter tubes. The liquid pressure drop associated with the liquid flow through the bed creates the force to transport the crystals through the column. A steering pump can be used to recycle filtrate into the top of the wash column to alter the transport force without needing to change the feed slurry. At the bottom of the wash column the crystals are scraped off by a rotating knife, and thus, enters the reslurry chamber. A stream of the pure melt is circulated through the reslurry chamber and transports the crystals through a heat exchanger, where the crystals are melted. The major part of the pure melt, which is the product, then leaves via the product valve.

A small excess pressure is created in the reslurry chamber by the product valve, so that the residual part of the melt is forced back into the column to perform a countercurrent washing action. The temperature of this pure wash-liquid equals the melting point of the material and will therefore crystallize on the downward moving crystals, which are still at

Correspondence concerning this article should be addressed to L. van Oord-Knol at this current address: DSM Research, Centre for Particle Technology, P.O. Box 18, 6160 MD Geleen, The Netherlands. Current address of O. S. L. Bruinsma, SASOL Centre for Separation Technology, Potchefstroom University for CHE, P.B. X6001, Potchefstroom 2520, Republic of South Africa.

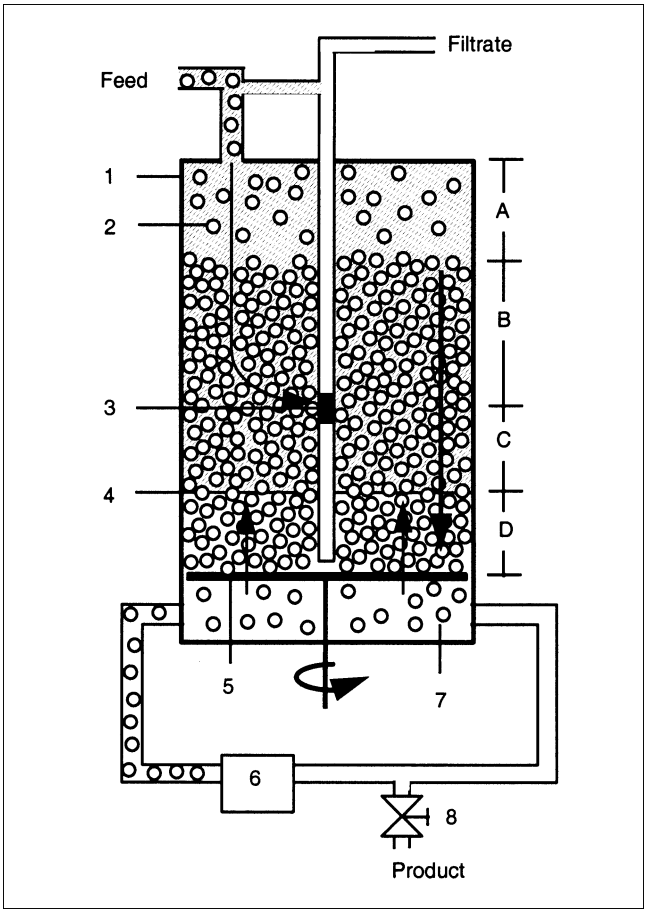

Figure 1. Principle of a hydraulic wash column.

1 = Column wall; 2 = moving crystal; 3 = filter in filter tube; 4 = wash front level; 5 = rotating knife; 6 = melter; 7 = reslurry chamber; 8 = product valvue. A = slurry section; B = filtration section; C = stagnant section; D = wash section.

feed temperature. In this way the wash liquid solidifies before it is lost via the filter tubes and forms a sharp wash front, which marks a considerable decrease in porosity and permeability. When hydraulic wash columns are used in nonmelt applications, the wash liquid will not solidify on the crystals and is therefore lost via the filters. Apart from the recrystallization, the basic principles for the solid–liquid separation and washing step are identical, so that theories developed for wash columns in melt crystallization can be applied to solution crystallization as well.

The main processes taking place in the wash column are filtration, displacement washing, and solidification. An important phenomenon in filtration processes is compression or consolidation of the filter cake, due to the forces exerted on the crystal bed. Due to these forces, the particles can rearrange or deform, which causes a decrease in porosity and permeability. For very compressible materials, the consolidation may be so large that an impermeable layer of material is formed when the pressure drop over the filter cake is too high. In fact the compressibility of the crystal bed determines the effectiveness of the filtration process and the optimal or even possible operating conditions (Svarovsky, 1990; Tiller and Yeh, 1987; Kamst et al., 1997a).

Compression of the crystal bed during the operation of a hydraulic wash column leads to a decrease in permeability of the packed bed both above and below the wash front. As a result, the pressure level in the wash column has to be increased to facilitate washing of the bed and to maintain transport of the packed bed. In previous research, models were presented to calculate the compressive stress profile in the wash column. However, in these models the compressibility of the crystal bed was not taken into account (Jansens et al., 1994a; Schneiders and Arkenbout, 1986).

The objective of this article was to evaluate the effect of the compressibility of a packed crystal bed on the performance of a hydraulic wash column. Therefore, a steady-state model of the wash column was extended to describe the consolidation of the bed in relation to the production rate of the wash column. The compressibility coefficients of the bed that are needed for the model calculations were determined from the porosity profile and the liquid-pressure profile, which were measured inside an operating wash column.

Modeling

Compressive stress in a hydraulic wash column

The stress distribution in a bed of particulate material with interstitial liquid flow is often described with the help of the effective stress. This is a useful simplification of the way in which the stress on the solid is transferred through the solid matrix (Tiller et al., 1987b; Atkinson, 1993). The effective stress is used to calculate the compressive stress profile in the wash column.

Assuming liquid flow in the axial direction only, a force balance over a horizontal slice of the crystal bed in the column (Figure 2) results in the following equation

$$\frac{d\sigma(h)}{dh} = -\frac{dp_1(h)}{dh} + (1-\epsilon)(\rho_s - \rho_l)g - \frac{4}{D}\tau_w(h) \quad (1)$$

The density difference between the mother liquor and the crystals is usually small for organic crystals, and the buoyancy term is therefore neglected in the remainder of the analysis.

According to the theory of Janssen (1895), the shear stress at the wall τ_w (Pa) can be calculated from the radial compressive stress σ_r (Pa), the wall friction coefficient μ_w and the ratio between radial and axial stress, K

$$\tau_w(h) = \sigma_r(h)\cdot\mu_w = \sigma(h)\cdot\mu_w\cdot K = K_f\cdot\sigma(h) \quad (2)$$

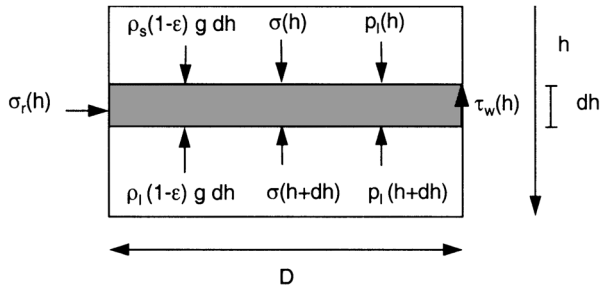

Figure 2. Stress distribution on a slice in the packed bed.

The wall friction coefficient and the stress ratio, K, are often combined to give the friction factor, K_f. Several authors have presented methods to determine the friction factor, K_f, in the wash column (Schneiders and Arkenbout, 1986; Jansens et al., 1994a; van Oord-Knol, 2000).

The liquid pressure drop over the cake in the wash column can be calculated with Darcy's law, which gives a linear relation between the pressure drop over the cake and the flow through the cake. The validity of Darcy's law for the calculation of the liquid-pressure drop in a hydraulic wash column is discussed in the Appendix. Since in a hydraulic wash column both the liquid and the solid move, the solid velocity has to be taken into account to calculate the superficial liquid velocity (Shirato et al., 1969), which transforms Darcy's law into

$$\frac{dp_l(h)}{dh} = -\frac{\eta\cdot\epsilon}{B}\left(\frac{\varphi_l}{A\cdot\epsilon} - \frac{\varphi_s}{A\cdot(1-\epsilon)}\right) \tag{3}$$

with ϵ the porosity of the cake defined as

$$\epsilon = \frac{\text{Volume of voids}}{\text{Volume of cake}} \tag{4}$$

The permeability, B (m^2), is a measure for the resistance of the filter cake. Usually the permeability is presented as a function of porosity. Coelho et al. (1997) give an overview of the relationships between these two quantities for packings. The well known Kozeny–Carman equation relates the permeability of the crystal bed to the porosity of the bed and the specific surface area, S_0 (m^2/m^3), of the particles that form the bed

$$B = \frac{\epsilon^3}{(1-\epsilon)^2}\frac{1}{kS_0^2} \tag{5}$$

The Kozeny constant, k, is about 5 for equally sized, spherical particles. For a polydisperse particle mixture or for nonspherical particles, k has to be determined experimentally. Equation 5 is of limited use for compressible materials, because the porosity and the Kozeny constant change when the bed is compressed (Svarovsky, 1990).

To calculate the compressive stress profile in the hydraulic wash column, the crystal bed is divided in three sections: the filtration section, the stagnant section, and the wash section, as shown in Figure 1. At the top of the crystal bed ($h = 0$), the compressive stress is 0, as the filtration length is zero. Since the crystal bed forms a continuous matrix throughout the wash column, the compressive stress at the end of a section is the start value of the compressive stress in the next section. When the liquid pressure profile in each section is known, the compressive stress profile can be calculated.

The liquid-pressure profile in the filtration section can be calculated from the flow rates, crystal concentration, and column dimensions using Eq. 6. For a compressible bed, the porosity and the permeability are functions of the position in the bed, because of the increasing compressive stress. The relations between the compressive stress and the porosity and permeability are given in Eqs. 11 and 12

$$\frac{dp_l(h)}{dh} = \frac{-\epsilon(h)\cdot\eta}{B(h)}\cdot\left(\frac{(1-\alpha)\cdot\varphi_{\text{feed}} + \varphi_{\text{steer}}}{\epsilon(h)\cdot A_c} - \frac{\alpha\cdot\varphi_{\text{feed}}}{(1-\epsilon(h))\cdot A_c}\right) \tag{6}$$

The direction of the superficial liquid velocity changes at the filters, and, therefore, the liquid pressure reaches its minimum, while the compressive stress reaches its maximum at the filters. It is assumed that the compression of the crystal bed is irreversible, so the porosity and the permeability in the stagnant zone (between the filters and the wash front) remain constant and equal to the porosity and permeability at the filters. It is further assumed that, in the steady state, there is no liquid flow in the stagnant zone. The movement of the crystal bed causes a linear liquid-pressure drop, which is calculated as follows

$$\frac{\Delta P_{l,st}}{L_{st}} = \frac{-\epsilon_{st}\cdot\eta}{B_{st}}\cdot\left(-\frac{\alpha\cdot\varphi_{\text{feed}}}{(1-\epsilon_{st})\cdot A_c}\right)\quad B_{st} = B(\text{filter}) \tag{7}$$

At the wash front, the wash liquid crystallizes on the cold crystals, which causes a steep decrease in the porosity and permeability. The amount of wash liquid that crystallizes is equal to the cooling capacity of the crystals. Assuming that all the wash liquid solidifies on the cold crystals, the porosity in the wash section and the wash liquid flow can be calculated. The porosity and permeability remain constant throughout the wash section, while the compressive stress decreases in the direction of the bed movement

$$\frac{\Delta P_{l,ws}}{L_{ws}} = \frac{-\epsilon_{ws}\cdot\eta}{B_{ws}}\cdot\left(-\frac{\varphi_{wl}}{\epsilon_{ws}\cdot A_c} - \frac{\left(\alpha\cdot\varphi_{\text{feed}} + \varphi_{wl}\cdot\frac{\rho_l}{\rho_s}\right)}{(1-\epsilon_{ws})\cdot A_c}\right) \tag{8}$$

with

$$\epsilon_{ws} = \epsilon_{st} - (1-\epsilon_{st})\cdot\frac{c_P\cdot(T_{\text{melt}} - T_{\text{feed}})}{\Delta H_m} \tag{9}$$

$$\varphi_{wl} = \alpha\cdot\varphi_{\text{feed}}\cdot\frac{c_P\cdot(T_{\text{melt}} - T_{\text{feed}})}{\Delta H_m}\cdot\frac{\rho_s}{\rho_l} \tag{10}$$

With this set of equations, it is possible to calculate the compressive-stress profile and the liquid-pressure profile in the wash column, when the relations between porosity and permeability and compressive stress are known.

Compressibility

To incorporate the compressibility of the bed into the model, the porosity and the permeability of the crystal bed have to be related to the compressive stress. A large amount of empirical relations are presented in both the soil mechan-

ics literature (van Impe, 1999), and in the filtration literature. Tiller and Yeh (1987) and La Heij et al. (1996) presented the following equations to describe the porosity and permeability of compressible particulate beds in filtration processes

$$\epsilon = \epsilon_0 \left(1 + \frac{\sigma}{\sigma_a}\right)^{-\lambda} \tag{11}$$

$$B = B_0 \left(1 + \frac{\sigma}{\sigma_a}\right)^{-\delta} \tag{12}$$

This type of equation is called constitutive, which means that the parameters are material dependent. Here, ϵ_0 and B_0 are the porosity and permeability at zero stress, and λ and δ are the compressibility coefficient for the porosity and the permeability, respectively. When these compressibility coefficients are equal to zero, the bed is incompressible. The term σ_a is an empirical scaling parameter without physical meaning (Tiller and Yeh, 1987). Equations 11 and 12 are used to describe the compressibility in the wash column. It is stressed that these are empirical relations and are only valid in a limited stress range, so predicted values for the permeability and the porosity outside this stress range have to be used with caution. A more theoretical determination of the mechanical properties of porous media can be found in Poutet et al. (1996).

The constitutive equations presented here assume that the material shows elastic deformation, which means that it deforms instantaneously when a stress is applied. When time-dependent consolidation, that is, creep, plays a role, the material behaves viscoelastic or viscoplastic. In soil mechanics and expression processes, creep has to be taken into account, as the material is subject to a load for a period, which is on the same order of magnitude as the time constant for creep (Kamst et al., 1997b; La Heij et al., 1996). In a hydraulic wash column, the residence times are short in comparison with phenomena in soil mechanics. Furthermore, there is a constant liquid-pressure gradient over the whole wash column, while creep will only dominate the consolidation rate of a bed, when the pressure drop has become negligible. It is therefore assumed that creep can be neglected in a wash column.

Experimental Procedure

Hydraulic wash column

The TNO-Thijssen-type hydraulic wash column that was used for the experiments is 15.6 cm in diameter and contains six filter tubes with an outer diameter of 2 cm. The filters are 3 cm high and are positioned 28 cm above the knife. The wash column is fed continuously from a 70-L scraped cooling crystallizer, that produces *p*-xylene crystals from a mixture of xylenes. For some experiments the crystal-size distribution was determined by sieve analysis. The mass-based mean diameter varied between 805 and 1350 μm.

The filtrate, product, and steering flow were measured with positive displacement meters and recorded with a PC. The pressures in the feed inlet, in the filtrate outlet, and in the melting circuit were recorded as well. The position of the wash front was visualized by adding a minor amount of red dye to the xylene mixture and was recorded manually, together with the length of the crystal bed. The range of process conditions used is given in Table 1.

Table 1. Range of Process Conditions During Experiments

Feed flow (L/h)	200–800
Crystal concentration (v/v)	0.04–0.14
Steering flow (L/h)	0–850
Product flow (L/h)	20–95
Top pressure (barg)	0.6–4.5
Filter pressure (barg)	0.04–0.4
Bottom pressure (barg)	0.4–1.6
Bed level above scraper (cm)	40–80
Wash front level above scraper (cm)	4–23

Determination of compressibility data

The compressibility coefficient of a particulate material can be determined in a so-called compression permeability cell (CP-cell), or in a filtration experiment, where the porosity and liquid pressure profiles are measured as a function of time (Svarovsky, 1990; Tiller et al., 1972; Chase and Willis, 1992; Shirato et al., 1985). In a CP-cell, a mechanical load is applied on the cake with help of a movable perforated piston. The cake porosity and permeability are measured as a function of the applied load. Application of a CP-cell in melt crystallization is troublesome, since the temperature of the slurry is critical: small temperature changes already induce large changes in crystal concentration and size distribution, and, thus, in the structure of the crystal bed under examination. Therefore, it was decided to determine the compressibility of the cake *in situ*, with help of porosity and liquid-pressure profiles in the wash column.

The porosity profile was determined from the product flow rate and the crystal velocity, that was measured at the wall of the column by following a single crystal on its way down through the glass column. The porosity of the crystal bed is related to the product flow, since the total flow of crystals through the column is constant and equals the liquid-product flow φ_p (m^3/s), when the wash column operates at a steady state. At any position in the column the velocity of the crystal bed, the porosity, and the product flow are therefore related via a mass balance as follows

$$\varphi_p \cdot \rho_l = v_s * (1 - \epsilon) * A_c * \rho_s \tag{13}$$

To determine the liquid pressure as a function of the position in the crystal bed, a stainless-steel tube with a small diameter was filled with liquid and was inserted in the hydraulic wash column, as shown in Figure 3. The thin tube was connected to a calibrated pressure transducer (P) with a multimeter, and can be moved up and down through the top flange of the wash column to determine the total liquid-pressure profile. To prevent the capillary from clogging with crystals when it is moved up and down, the lower end was closed and several small holes were made in the circumference of the capillary near the bottom. The tube was filled with ethylene glycol to prevent the crystallization of liquid in the tube. Tubes with an outer diameter of 3 mm and of 2 mm were used, while the length of the tubes varied between 0.95 and 1.15 m. It was

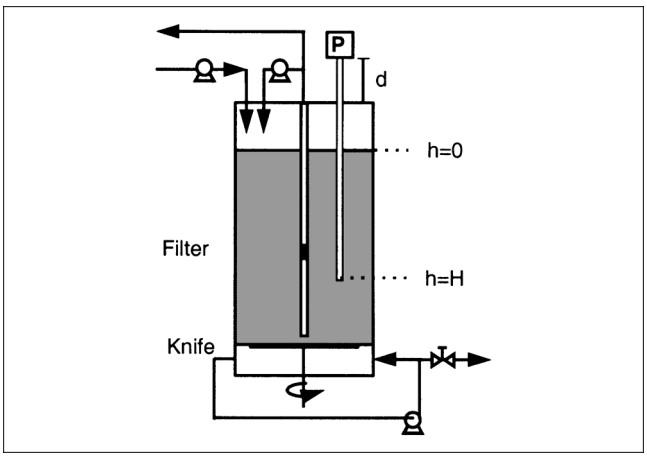

Figure 3. Small-diameter tube in the hydraulic wash column to measure local liquid pressure.

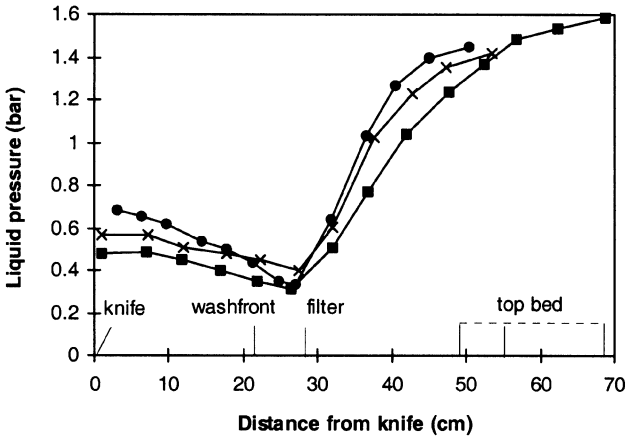

Figure 5. Measured liquid pressure profiles in the hydraulic wash column, for beds of 69 cm (■), 54 cm (×), and 49 cm (●).

demonstrated that the introduction of the tube did not change the stress profiles significantly (van Oord-Knol, 2000). The data presented have been corrected for the differences in hydrostatic pressure caused by the different lengths of the capillaries.

Results and Discussion

Porosity profiles

The porosity profiles are determined from crystal velocity profiles, which were measured at several production rates. The porosity decreases from the top of the crystal bed to the filters, as shown in Figure 4, while the three chosen representative profiles scatter around the same curve. To calculate the porosity below the wash front, the volume flow of the crystals was corrected for the wash liquid that is crystallized on the crystals. The porosity decrease at the wash front amounts to 0.04 (Eq. 9). In Figure 4, this decrease is not visible due to the scatter in the porosity.

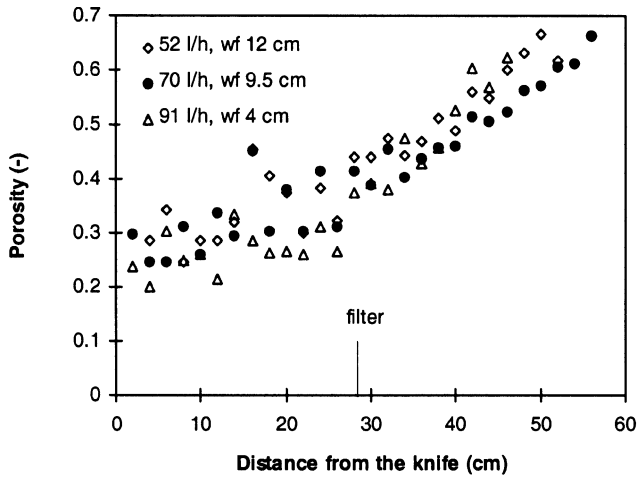

Figure 4. Porosity for three production rates and wash-front levels (*wf*).

The porosity profiles below the wash front are corrected for crystallization at the wash front.

The determined porosity in the top of the crystal bed is high for a packed bed. The reported values can be slightly overestimated, because the porosity can only be determined at the wall of the column with the method used, and the porosity at the wall is usually somewhat higher than in the center of a packed bed (Vortmeyer and Schuster, 1983). The advantage of the method used, however, is that it does not disturb the bed with inserted probes. Another reason for the relatively high porosity at the top of the bed may be the strong movement of the crystals in the entrance zone just above the crystal bed, which is presumably caused by the velocity of the feed flow that is forced into the wash column.

Liquid-pressure profiles

Figure 5 shows three representative liquid-pressure profiles measured under different process conditions in the wash column. The measured liquid pressure decreases from the top of the crystal bed to the filters. The liquid-pressure gradient in the top of the crystal bed becomes steeper in the direction of the filter tubes and does not decrease linearly, as is assumed in the work of Jansens et al. (1994a). The measured profiles confirm that the bed is compressible: due to the decreasing porosity, both the resistance of the bed, and the liquid-pressure drop increase at greater distances from the top of the bed.

From the filters to the knife the measured liquid pressure increases, which agrees with the fact that wash liquid is introduced at the bottom of the column and flows in the direction of the filters. It is remarkable that there is hardly any difference in the liquid pressure gradient in the wash section and in the stagnant zone. It is assumed that in a steady state there is a wash liquid flow in the wash section, while in the stagnant zone, only the crystal bed is moving. This should result in a steeper liquid-pressure gradient in the wash section. This discrepancy may be caused by minor fluctuations in the level of the wash front: a rising wash front causes the mother liquor to flow to the filters, when it is replaced by the wash liquid, which causes the liquid-pressure gradient. It was not possible to investigate this more precisely, because the wash front was

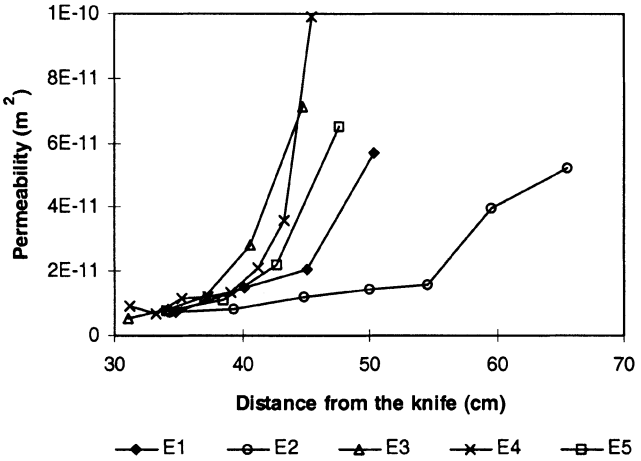

Figure 6. Permeability profiles in the filtration section of the wash column.

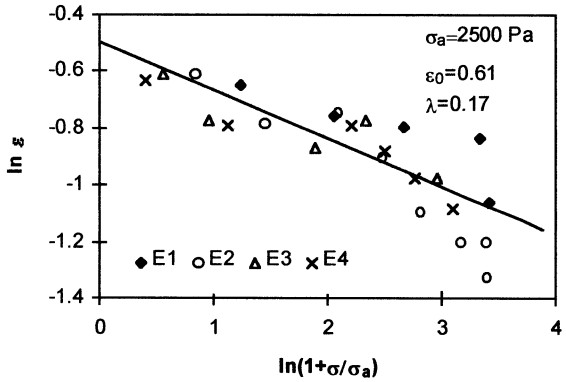

Figure 7. Compressibility coefficient λ, from porosity and liquid pressure.

relatively high (about 20 cm) in most of the liquid-pressure measurements.

The liquid-pressure measurements were carried out at a single radial position in the column, so no information was obtained on the validity of the one-dimensional approach for the liquid pressure and flow profiles. However, the aspect ratio of the wash column, defined as the ratio between the distance the liquid has to move in the axial and radial directions, ranges from 10 to 25, depending on the length of the packed bed. In addition, six filters are positioned in the column, so the radial velocity at the filters is about 1.5 times the velocity in axial direction. Due to the short distance in the radial direction, the pressure drop caused by radial liquid flow will be relatively small compared to the pressure drop in the axial direction.

Permeability profiles

The measured liquid-pressure profiles can be used to determine the permeability B as a function of the position in the bed (Eq. 3). Figure 6 shows the permeability in the top section of the wash column for five experiments (E1–E5). These permeability profiles will be used in the next section to determine the compressibility coefficients. Going from the top of the bed to the filters, a tenfold decrease in the local permeability was measured. Since the crystals in the top section are suspended in the mother liquor at adiabatic conditions, no major freezing or melting phenomena occur, so the measured effect can be attributed to compression of the bed.

The local permeability at the filters is, thus, considerably lower than the average permeability in the top section, and this may help to explain the unexpectedly large ratio between the average permeability above and below the wash front, as reported by Jansens et al. (1994b). These authors found a ratio between the average permeability above and below the wash front that amounted to 7, and again in experiments E1 to E5 a ratio was found that varied from 3.6 to 6. However, at a typical temperature difference of 6.5°C, a ratio of 1.6 would be expected when, for an incompressible bed, the porosity decrease due to crystallization of the wash liquid (Eq. 9) is combined with the Kozeny–Carman relation (Eq. 5).

Since in experiments E1 to E5 the local permeability at the filters is 1.9 times lower than the average permeability in the top section, it is shown that due to compressibility of the bed, predictions of the permeability in the wash section have to be based on the local permeability at the filters and not on the average permeability of the top section.

Compressibility coefficient: Porosity decrease

To determine the compressibility coefficient for the porosity decrease, we use the measured liquid-pressure profiles and the measured porosity profiles. In four experiments these profiles were determined immediately after each other, so that the process conditions can be considered to be equal. When Eqs. 1 and 2 are combined, and the buoyancy force is neglected, the liquid-pressure profile can be used to calculate the compressive stress profile in the crystal bed as follows

$$\frac{d\sigma(h)}{dh} = -\frac{dp_l(h)}{dh} - \frac{4K_f}{D_h}\sigma(h) \tag{14}$$

A value of 0.09 is used for the friction factor (van Oord-Knol, 2000). The hydraulic diameter, D_h, of the wash column is $7.95 * 10^{-2}$ m, and the compressive stress at the top of the bed is zero. A plot of ln ϵ(h) vs. ln $[1+\sigma(h)/\sigma_a]$ is used to obtain the compressibility coefficient, λ, which is the slope of this plot.

Figure 7 shows the plots for the four experiments, and Table 2 summarizes the values for the compressibility and the porosity at zero stress, ϵ_0. This ϵ_0 is an extrapolated value determined from the intercept of the compressibility plot; for the xylene slurry, it amounted 0.61 ± 0.10. The compressibil-

Table 2. Compressibility Coefficients with Main Process Conditions During Experiments

Exp.	$\Delta P_{l,\text{filt}}$ (bar)	L_{filt} (cm)	Feed (L/h)	ϵ_0	λ	$B_0 \times 10^{11}$ (m^2)	δ
E1	1.26	54	494	0.63	0.14	11	0.88
E2	1.46	69	366	0.71	0.26	9.3	0.80
E3	1.24	47	597	0.55	0.12	10	0.95
E4	1.0	47	627	0.56	0.14	8.2	0.80
E5	1.06	49	471	—	—	11	0.91

ity for the porosity, λ, determined from a combination of the porosity and liquid-pressure profiles, was 0.17 ± 0.09. The line in Figure 7 represents the logarithm of both sides of Eq. 11, using $\lambda = 0.17$ and $\epsilon_0 = 0.61$. Note that a high value of ϵ_0 is compensated for by a high value of λ, which probably has a numerical fitting reason rather than a physical one. The same holds for B_0 and δ.

Compressibility coefficient: Permeability decrease

Since theoretical relations between porosity and permeability are considered to be inadequate for compressible beds, the compressibility coefficient, δ, which relates permeability to compressive stress, was measured separately. For this reason, the local permeability $B(h)$ was determined from the local liquid-pressure drop, according to Eq. 3. The compressive stress was again calculated with Eq. 14 to obtain a set of permeability–compressive-stress data. Figure 8 shows the plot from which the compressibility coefficient, δ, and the permeability at zero stress, B_0, were determined with linear regression. These values are summarized in Table 2 for five experiments. The compressibility coefficient, δ, for the *p*-xylene crystal bed amounted to 0.87 ± 0.08, and the permeability at zero stress, B_0, amounted to $9.9*10^{-11}$ m^{-2}. The line in Figure 8 describes the logarithm of both sides of Eq. 12, using these values.

Kozeny – Carman for compressible crystal beds

If the permeability can be accurately calculated from the porosity, the porosity at zero stress and the compressibility coefficient for the porosity would suffice to calculate the pressure in the wash column from the process flow rates. The Kozeny–Carman equation is often used to calculate the permeability from the porosity, but is considered to be inaccurate for compressible cakes (Svarovsky, 1990). This notion was investigated for the experiments described in the previous section. In Table 3 the measured liquid-pressure drop is compared with the pressure drop that was calculated from the permeability and compressibility coefficient, λ, and with the pressure drop calculated from the porosity, Kozeny–Carman equation, and compressibility coefficient, δ, as given in Table 2. The liquid-pressure drop was measured and calculated for

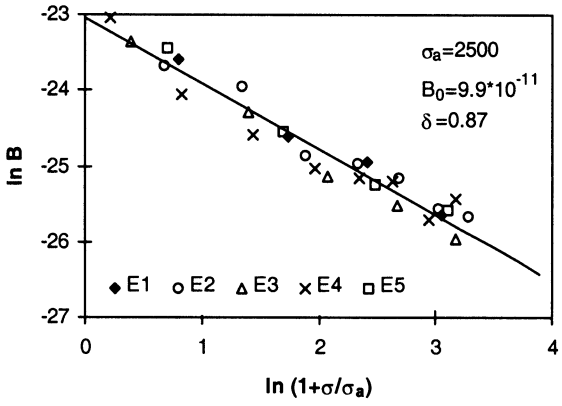

Figure 8. Compressibility coefficient δ, from liquid pressure.

Table 3. Measured and Calculated Liquid Pressure Drop Based on Permeability or Porosity Used in the Kozeny–Carman Equation

Exp	$\Delta P_{l,\text{measured}}$ (bar)	$\Delta P_{l,\text{permeability}}$ (bar)	$\Delta P_{l,\text{porosity}}$ (bar)
E1	0.81	0.755	0.460
E2	1.08	0.906	1520
E3	0.802	0.686	0.216
E4	0.754	0.893	0.403

that section of the wash column for which the local permeability and porosity were determined. The calculated liquid-pressure drop deviates from the measured pressure drop. For the calculation based on the permeability, this deviation varies from 7% to 20%, while for the calculations based on the porosity, this deviation is 47% up to unrealistically high values. This large error in the prediction is explained by the low accuracy of the compressibility coefficient for the porosity. Since the permeability could be determined more accurately than the porosity, the compressibility coefficient is more accurate, which means the pressure-drop predictions are more accurate.

When the average values for the compressibility coefficients and ϵ_0 and B_0 are used to calculate the liquid-pressure drop for a range of feed flow rates and bed heights, the difference between the liquid-pressure drops is small for low flow rates, but increases with increased feed rates, as shown in Figure 9. For a wide range of process conditions, however, the two methods used to calculate the liquid-pressure drop give only slightly different results. This indicates that for the porosity range prevailing in the wash column ($0.35 < \epsilon < 0.65$), the two empirical relations (Eqs. 11 and 12) presented in the theory correspond very well with common porosity–permeability correlations that use a power law and with the Kozeny–Carman equation. Combining Eqs. 11 and 12 gives

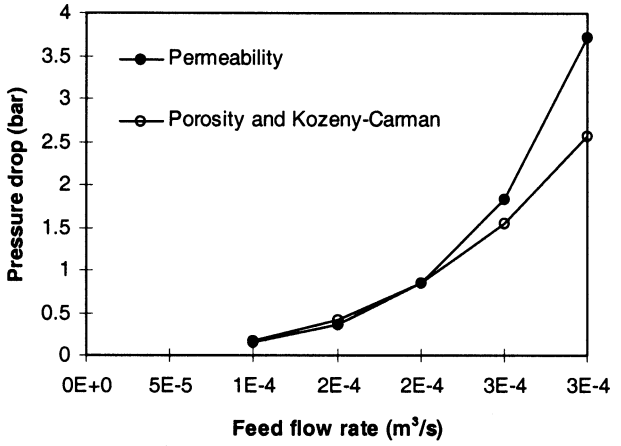

Figure 9. Liquid pressure drop in compressible bed for increasing flow rates calculated from the permeability, using B_0 and λ and from the porosity using ϵ_0 and δ.

$L_{\text{bed}} = 50$ cm; $\alpha = 0.15$; $\varphi_{\text{steer}} = 0$ m^3/s; $\epsilon_0 = 0.61$; $\lambda = 0.17$; $B_0 = 9.9 \times 10^{-11}$ m^2; $\delta = 0.87$.

Eq. 15

$$B = B_0\left(\frac{\epsilon}{\epsilon_0}\right)^{\delta/\lambda} \tag{15}$$

The experimental compressibility coefficients then result in an exponent of $0.87/0.17 = 5.1$, which is in agreement with the Kozeny–Carman equation, because in the relevant porosity range, the factor $\epsilon^3/(1-\epsilon)^2$ is roughly proportional to ϵ^5. The experimental exponent of 5.1 is also in agreement with the values ranging from 4.15 to 5.5, as presented by several authors (Coelho et al., 1997).

Compressibility and wash-column performance

To investigate the relation between the compressibility of a packed bed and the production rate of the wash column, simulations were carried out with the model described. In the simulations the length of the bed and the position of the wash front were kept constant by adjusting the steering flow and the product control valve, as is done in real experiments. The steering flow was adjusted such that the stress at the knife is zero, which means that the bed does not rest on the knife.

For the simulations it was assumed that the porosity and permeability at the top of the bed, that is, ϵ_0 and B_0, are not influenced by the process conditions. This is a simplification, which neglects the influence of the feed rate, the position of the top of the crystal bed, and the crystal concentration, which all have an effect on the initial packing of the crystals. The properties of the compressible and the incompressible crystal bed are summarized in Tables 4 and 5, respectively. For the compressibility coefficients, the values determined in the preceding subsections were used. For the incompressible bed, representative average values of the permeability and porosity were used to calculate the pressure with increasing production rates.

For the given process conditions and the defined bed height and wash-front height (Table 6), the calculation starts with the calculation of the compressive-stress profile, the liquid-pressure profile, and the porosity profile in the filtration section of the crystal bed, using Eqs. 6, 11, and 12 to solve

$$\frac{d\sigma}{dh} = -\frac{dp_{l,\text{filt}}}{dh} - \frac{4K_f}{D_h}\sigma \tag{16}$$

This gives the values for the porosity and permeability at the filters, which are then used to calculate the porosity and permeability in the wash section. The position of the wash front is kept constant. In practice, this is accomplished by closing or opening the product valve to provide the pressure needed to keep the wash front constant. In the calculations, the pressure drop over the bottom section follows directly from the bed and liquid velocity and the wash-front height.

Table 4. Properties of the Compressible Crystal Bed

ϵ_0	0.61
B_0 (m^2)	9.9×10^{-11}
λ	0.17
δ	0.87
K_f	0.09

Table 5. Properties of the Incompressible Crystal Bed

ϵ	0.40
B (m^2)	1.6×10^{-11}
K_f	0.09

Table 6. Standard Process Conditions

L_{bed} (m)	0.50
L_{wash} (m)	0.15
φ_{feed} (m^3/s)	9.6×10^{-5}
α (m^3/m^3)	0.15

To investigate the effect of the compressibility on the attainable production rate, the production rate was increased, which can be done by increasing the feed flow to the column or by changing the crystal content of the feed. Obviously, this gives the same result in the calculations for a given production rate, since the steering flow is adapted, such that the crystal content entering the column after mixing with the feed remains constant.

Figure 10 shows that for an incompressible bed the pressure at the top increases linearly with the production rate. It further shows that the compressibility of the crystal bed can have a large influence on the stress level in the wash column: for the simulated compressible bed, the pressure at the top of the column increases exponentially with increasing production rates. High throughputs are, thus, not realistic for very compressible beds, because of the high feed pressure levels on the one hand, and because of the high wash pressures on the other. This indicates that the compressibility of the bed determines the operating window of the hydraulic wash column. This operating window can be enlarged by changing the position of the wash front; for a lower wash front, a lower wash pressure is needed, and, thus, a lower pressure at the top. For a production rate of 8185 kg/m^{2}h, a wash section of 10 cm would give a pressure of 12 bar at the top, while for a wash section length of 15 cm, 19 bar was calculated.

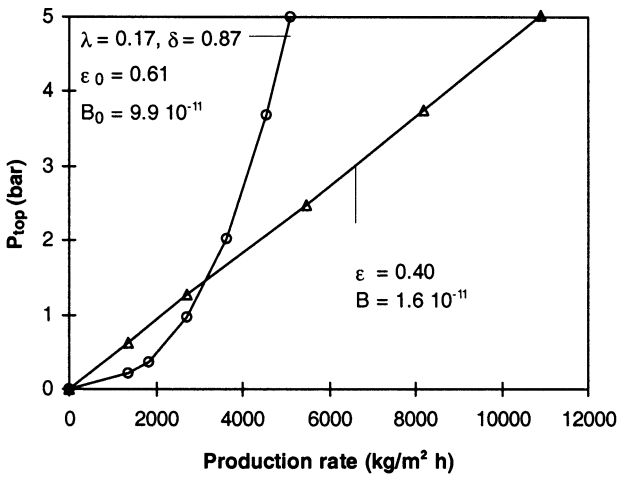

Figure 10. Simulated pressure in the wash column for increasing production rates for a compressible and an incompressible bed.

$L_{\text{bed}} = 50$ cm; $L_{\text{wash}} = 15$ cm.

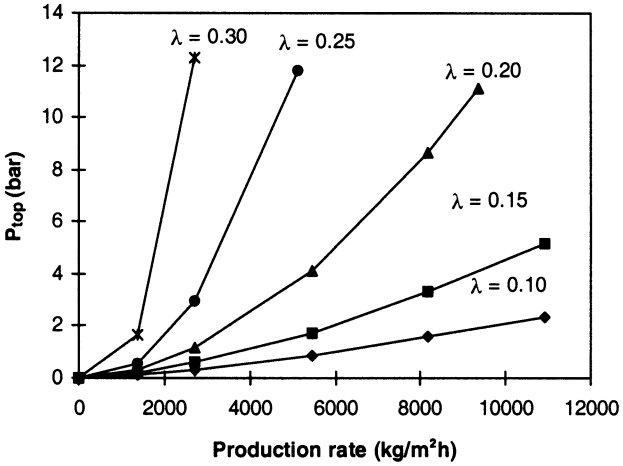

Figure 11. Simulated pressure in the wash column for increasing production rates for various compressibility coefficients λ.

$L_{bed} = 50$ cm; $L_{wash} = 15$ cm.

It has to be mentioned here that the compressibility coefficients may change when the crystal properties change. Changes in the particle size and/or the shape, but also the compressibility of the solid itself, will influence the compressibility and the specific production capacity of the wash column. The effect of the value of the compressibility coefficient was examined by calculating the pressure for increasing production for various values for the compressibility coefficient for the porosity, λ. To calculate the permeability of the bed, the Kozeny–Carman equation and the porosity are used, instead of the compressibility for the permeability, δ. It was shown that at higher feed rates the pressure drop is underestimated this way. Figure 11 shows that for higher compressibility coefficients, the pressure at the top rises more with increasing production rates. Therefore, the higher the compressibility, the smaller the operating window of the wash column.

Conclusions

The compressibility of a packed bed limits the capacity of a wash column. This phenomenon was therefore quantified and modeled rigorously. For para-xylene crystals in a hydraulic wash column, the compressibility was determined with the help of *in situ* measured porosity and liquid-pressure profiles. The porosity of the bed decreases from 0.65 to 0.3 during transport of the bed. This decrease is associated with a decrease in the local bed permeability by a factor of 10. This decrease in porosity and permeability was characterized with a compressibility coefficient for the porosity, λ, that amounted to 0.17 ± 0.09, and with a compressibility coefficient for the permeability, δ, that amounted 0.87 ± 0.08.

The compressibility of the packed bed largely explains the fact that the ratio between the permeability in the top of the crystal bed and in the wash section is higher than the permeability ratio, that is expected based on crystallization of the wash liquid.

Simulation of the effect of the compressibility on the capacity of the wash column shows that the production capacity may be limited for compressible beds, because the liquid pressure at the top increases more than linearly with the production rate. The higher the compressibility, the larger the effect, that is, the higher the liquid pressure at the top of the column.

Acknowledgment

The authors thank the NOVEM, and especially A. Kok, for the financial support of the project. The authors also thank D. Verdoes and M. Nienoord from TNO-MEP for the fruitful discussions and the use of the pilot plant. P. Huisjes and H. van der Meer are thanked for their skilled assistance during the experiments.

Notation

A = cross-sectional area, m^2
A_c = wetted cross-sectional area, m^2
B = permeability, m^2
c_P = specific heat of the solid phase, kJ/kg·K
D = diameter, m
D_h = hydraulic diameter, m
g = gravity constant, m/s^2
h = vertical coordinate, m
ΔH_m = latent heat of fusion, kJ/kg
K_f = friction factor
K = ratio between radial and axial stress
k = Kozeny constant
L = total length of a section, m
p_l = liquid pressure, Pa
P_s = maximum compressive stress, Pa
S_0 = specific surface area, m^2/m^3
T_m = melt temperature of the crystals, °C
T_{feed} = temperature of the feed, °C
v = velocity, m/s
v_{sup} = superficial liquid velocity, m/s

Greek letters

α = crystal fraction in the feed
δ = compressibility coefficient for the permeability
λ = compressibility coefficient for the porosity
ϵ = porosity
η = viscosity, Pa·s
φ = flow rate, m^3/s
ρ = density, kg/m^3
σ = compressive stress, Pa
μ_w = wall-friction coefficient
τ_w = shear stress at the wall, Pa

Subscripts

filt = filtration section
filter = at the filter
l = liquid
p = product
0 = at zero stress
s = solid
st = stagnant zone
steer = steering flow
wl = wash liquid
ws = wash section

Literature Cited

Arkenbout, G. J., *Melt Crystallization Technology*, Technomic, Lancaster, PA (1995).

Atkinson, J., *An Introduction to the Mechanics of Soils and Foundations; Through Critical State Soil Mechanics*, McGraw-Hill, London (1993).

Chase, G. G., and M. S. Willis, "Compressive Cake Filtration," *Chem. Eng. Sci.*, **47**, 1373 (1992).

Coelho, D., J.-F. Thovert, and P. M. Adler, "Geometrical and Transport Properties of Random Packings of Spheres and Aspherical Particles," *Phys. Rev. E.*, **55**, 1959 (1997).

Jansens, P. J, O. S. L. Bruinsma, and G. M. van Rosmalen, "Compressive Stresses and Transport Forces in Hydraulic Packed Bed Wash Columns," *Chem. Eng. Sci.*, **49**, 3535 (1994a).
Jansens, P. J, O. S. L. Bruinsma, G. M. van Rosmalen, and R. de Goede, "A General Control Strategy for Hydraulic Packed Bed Wash Columns," *Trans. Inst. Chem. Eng.*, **72**, 695 (1994b).
Janssen, H. A., *Z. Ver. Dtsch. Ing.*, **39**, 1045 (1895).
Kamst, G. F., O. S. L. Bruinsma, and J. de Graauw, "Permeability of Filter Cakes of Palm Oil in Relation to Mechanical Expression," *AIChE J.*, **43**, 673 (1997a).
Kamst, G. F., O. S. L. Bruinsma, and J. de Graauw, "Solid-Phase Creep During the Expression of Palm-Oil Filter Cakes," *AIChE J.*, **43**, 665 (1997b).
La Heij, E. J., P. J. A. M. Kerkhof, K. Kopinga, and L. Pel, "Determining Porosity Profiles During Filtration and Expression of Sewage Sludge by NMR Imaging," *AIChE J.*, **42**, 953 (1996).
Poutet, J., D. Manzoni, F. Hage-Chehade, C. J. Jacquin, M. J. Boutéca, J.-F. Thovert, and P. M. Adler, "The Effective Mechanical Properties of Random Porous Media," *J. Mech. Phys. Solids*, **44**, 1587 (1996).
Schneiders, L. H. J. M., and G. J. Arkenbout, "Developing a High Efficiency Wash Column," *Filtr. Sep.*, 304 (Sept./Oct. 1986).
Shirato, M., T. Murase, E. Iritani, and S. Nakatsuka, "Filter Cake Dewatering by Formation of Bentonite Skin Layer on Cake Surface," *J. Chem. Eng. Jpn.*, **18**, 372 (1985).
Shirato, M., M. Sambuichi, H. Kato, and T. Aragaki, "Internal Flow Mechanism in Filter Cakes," *AIChE J.*, **15**, 405 (1969).
Svarovsky, L., *Solid-Liquid Separation*, Butterworths, London (1990).
Tiller, F. M., and C. S. Yeh, "The Role of Porosity in Filtration," *AIChE J.*, **33**, 1241 (1987).
Tiller, F. M., C. S. Yeh, and W. F. Leu, "Compressibility of Particulate Structures in Relation to Thickening, Filtration and Expression. A Review," *Sep. Sci. Technol.*, **22**, 1037 (1987).
Tiller, F. M., S. Haynes, and W. M. Lu, "The Role of Porosity in Filtration VII. Effect of Side Wall Friction in Compression-Permeability Cells," *AIChE J.*, **18**, 13 (1972).
Van Impe, W. F., and P. van Impe, "Mechanical Properties of MSW and Considerations on Consolidation of Dredged Material," Conferenze di Geotechnica di Torino, Torino, Italy (1999).
Van Oord-Knol, L., "Hydraulic Wash Columns. Solid-Liquid Separation in Melt Crystallization," PhD Thesis, Delft Univ. of Technology, Delft, The Netherlands (2000).
Vortmeyer, D., and J. Schuster, "Evaluation of Steady Flow Profiles in Rectangular and Circular Packed Beds by a Variational Method," *Chem. Eng. Sci.*, **38**, 1691 (1983).

Appendix: Validity of Darcy's Law for the Wash Column

The linear relation between pressure drop and liquid velocity as assumed in Darcy's law is only valid for laminar flow. For higher Reynolds numbers, the Ergun equation should be used (Svarovsky, 1990)

$$\frac{\Delta P_l}{L} = 150 \cdot \frac{v_{\text{sup}} \cdot \eta}{x_{sv}^2} \cdot \frac{(1-\epsilon)^2}{\epsilon^3} + 1.75 \cdot \frac{v_{\text{sup}}^2 \cdot \rho_l}{x_{sv}} \cdot \frac{1-\epsilon}{\epsilon^3} \quad \text{(A1)}$$

To estimate the possible error that is made when using Darcy's law to calculate the liquid-pressure drop in the wash column, first the surface volume diameter was estimated from the average permeability in the top section and a porosity of 0.40, using the first part of Eq. A1. This x_{sv} varies from 70 μm to 150 μm. Then the superficial liquid velocity was calculated from the process conditions summarized in Table 1. The superficial velocity varies from 0.004 m/s to 0.017 m/s. With $\rho_l = 867$ kg/m^3 and $\eta = 0.68 \times 10^{-3}$ Pa·s, the contribution of both parts of Eq. A1 to the liquid-pressure gradient can be calculated. It appears that the first part of Eq. 1 determines 94.7% to 98.8% of the calculated liquid pressure gradient. The small error made is acceptable for the calculations in this work.

Manuscript received July 13, 2001, and revision received Dec. 17, 2001.